Investigation on Wavelength Multicasting Technology Based on XPM in a Highly Nonlinear Fiber

Minjie Wang[*1,2,3] Jian-Guo Zhang[4]

1.(State Key Laboratory of Transient Optics and Photonics, Xi'an Institute of Optics and Precision Mechanics, Chinese Academy of Sciences, Xi'an 710119, China)
2.(University of Chinese Academy of Sciences, Beijing, 100049, China)
3.(College of Sciences, Henan Agricultural University, Zhengzhou 450002, China)
4.(Department of Engineering and Design, London South Bank University, 103 Borough Road, London SE1 0AA, UK)

Abstract: All-optical wavelength conversion with multicasting is investigated in this paper, which is based on cross-phase modulation in a highly nonlinear fiber. With a pump-modulated light and only a single continuous-wave probe, wavelength multicasting is realized by appropriately controlling the powers of two beams. Our simulation work reveals that ten multicast channels can be obtained with their Q factors being larger than 6, if both pump and probe powers are properly selected. These wavelength channels of multicasting are positioned around the central wavelength of the probe on the blue-shifted and red-shifted sides. The central wavelength and the channel spacing can be affected by the wavelengths of the probe and the pump. The wavelength multicasting technique studied in this paper is simpler and can offer more multicast channels than that based on four-wave mixing.

Keywords: All-optical wavelength conversion; multicasting; cross-phase modulation; highly nonlinear fiber.

1. Introduction

All-optical wavelength conversion (AOWC) is a key technology for wavelength-division-multiplexing (WDM) networks [1–6], which enables wavelength switching and routing between channels and facilitates wavelength reuse to improve the operational flexibility in such networks [1–4], while reducing blocking probability. Recently, wavelength multicasting has been attracting considerable attention [4,7–9], as it can copy an optical signal at the given wavelength into multiple optical signals at different wavelengths and allows the transmission of the replicated signals at the corresponding wavelengths from a source node to multiple destination nodes simultaneously. As a result, WDM networks require a function of wavelength multicasting to support bandwidth-intensive applications such as video distribution and teleconference [4,7,8]. AOWC with multicasting can be accomplished by exploiting optical nonlinear mechanism in several materials, such as semiconductor optical amplifier devices [9], nonlinear silicon nanowires [10], and optical fibers [4,8,11,12]. Among various media and technologies, four-wave mixing (FWM) in an optical fiber is promising for AOWC with multicasting [4,8,12], because highly nonlinear fibers (HNLFs) and nonlinear photonic crystal fibers are commercially available and transparent to modulation format [4,8]. However, FWM relies on the phase-matching condition, and the conversion efficiency may be not high [1]. In addition, the flexibility of FWM-based wavelength conversion is also low [5].

In this paper, we investigate AOWC with multicasting based on cross-phase modulation (XPM) in a highly nonlinear fiber because of its easy implementation, low cost, ultrafast response, and

[*]Minjie Wang(✉)
e-mail: wmzk2002@163.com

suitability for integration with fiber-based systems. So far, XPM in an optical fiber has been mainly used for AOWC [5][14]. However, the research on fiber XPM-based wavelength multicasting has received less attention than that for AOWC. To efficiently support bandwidth-intensive applications, it is necessary to study the performance of fiber XPM-based wavelength multicasting in the WDM operation environment. At present, there is lack of research on the dependence of the number of multicast channels on the powers of a single probe and a single pump for the AOWC based on XPM in a HNLF. From the viewpoint of system design and practical applications, a simple technique is highly desired to implement wavelength multicasting with a large number of multicast channels. Until now, there is no report on the use of fiber XPM-based wavelength multicasting scheme employing only a single probe and a single pump to create a large number of multicast channels with satisfactory Q factors (e.g., $\geqslant 6$) by means of simply controlling both light powers. Therefore, we propose a simple method of wavelength multicasting to effectively provide multiple channels with $Q \geqslant 6$ by properly selecting the powers of a pump-modulated light and a single continuous-wave (CW) probe for XPM in a HNLF with no increase of system complexity and cost, as will be reported subsequently.

2. Simulation Setup

We carry out our simulation research work on XPM-based AOWC with multicasting by using the OptiSystem software. The schematic diagram is shown in Figure 1. In the simulation, a non-return-to-zero (NRZ) optical data signal at 10 Gbit/s is generated by modulating a strong CW light at a Mach–Zehnder modulator with an input 10Gbit/s electronic signal from a NRZ data pulse generator cascaded with a pseudo-random bit sequence generator. The obtained optical data signal is then used as a pump light with high power for XPM-based wavelength multicasting. The probe is a weak CW light that is combined with the pump-modulated light through a 3dB optical coupler. Two polarization controllers (PCs) at the inputs of a 3dB optical coupler are used to maximize the XPM effect by adjusting the states-of-polarization of the input lights. The probe and pump wavelengths are equal to λ_p and λ_s, respectively, where $\lambda_p \neq \lambda_s$. The combined lights are launched into a 1km highly nonlinear fiber (HNLF) to make XPM. The HNLF used in our simulation has a nonlinear-index coefficient of 5×10^{-20} m^2/W, an effective area of 10 μm^2, an attenuation of 0.5 dB/km, and a reference wavelength at 1550 nm [15]. The dispersion of the HNLF is equal to 5 ps/nm/km in the third simulation case and is set to 2 ps/nm/km in the other three cases. The dispersion slope of the fiber is 0.03 $ps/nm^2/km$ in the first three simulation cases, while being 0.07 $ps/nm^2/km$ in the last simulation case. Moreover, a bank of tunable band-pass filters (BPFs) with 0.2nm bandwidth are used at the HNLF output to select the wavelength-converted signals by individually filtering out the desired optical spectral components at multiple wavelengths on the red-shifted and blue-shifted sides of the XPM-broadened probe spectrum. An optical attenuator is placed at the input of each PIN photodetector. An electronic Bessel LPF with cut-off frequency of 7.5 GHz is also used at the output of each PIN photodetector to remove the out-of-band receiver noise. The bit error rate (BER) measurement is performed at the output of each optical receiver. The optical spectra of pump and probe lights can be measured by placing an optical spectrum analyzer at point A, B, or C.

3. Results and Discussions

3.1 Simulation case 1: Dispersion=2 ps/nm/km, dispersion slope=0.03 $ps/nm^2/km$, λs=1555 nm, and λp=1545 nm

Fig. 2 shows the optical spectra of the 1555nm pump light with power of 45 mW and the 1545nm probe light with power of 1 mW before entering the HNLF (point A in Fig. 1). Fig. 3 shows the optical spectra of both lights at the HNLF output measured at point B. Comparing Figs. 2 and 3, a peak appears at 1544.49 nm wavelength (marked as *a* in Fig. 3). The central wavelength of an optical BPF is tuned from 1543 nm to 1547 nm at 0.1 nm interval to filter out the wavelength-converted signals. The simulation results show that the converted signals cannot be obtained at most wavelength points, and these signals can be filtered out at 1544.49 nm (*a* point wavelength) and 1545 nm (probe

wavelength). Fig. 4 shows the wavelength-converted signals at 1544.49 nm after the BPF in time domain. Fig. 5 shows the eye diagrams at 1544.49 nm. In addition, the measured Q factor is 29.8, which indicates successful datum transfer to a new wavelength and complete wavelength conversion.

Increasing pump power results in broadened optical spectrum of the probe. When the probe power is increased to 5 mW (λp=1545 nm) and the pump power is fixed on 45 mW (λs=1555 nm), two peaks are shown, which are marked as point a at wavelength 1544.49 nm and point b at wavelength 1545.52 nm in Fig. 6. The BPF1, BPF2, and BPF3 central wavelengths are tuned to 1544.49, 1545.52, and 1545 nm, respectively, and the datum signals can be filtered out, which indicate datum transfer to three new wavelengths and complete wavelength conversion with multicasting. The ratio between the pump power and the probe power is fixed at 10. Similarly, when the probe power is increased to 10 mW and the pump power is increased to 100 mW, three peaks are found, which are marked as points a (at 1544.49 nm), b (at 1545.51 nm), and c (at 1543.98 nm) in Fig. 7. Fig. 8 shows the optical spectra when the pump power is 200 mW and the probe power is 20 mW. Fig. 9 shows the optical spectra when the pump power is 300 mW and the probe power is 30 mW. Comparing Figs. 6, 7, 8, and 9, the simulation results demonstrate that the pump and probe powers are increased, the probe optical spectrum becomes wider, and the number of peaks is increased.

In Fig. 9, at least nine peaks are prominent; these peaks are marked as points a, b, c, d, e, f, g, h, and i. Ten multicast channels can be obtained with their Q factors being larger than six. The central wavelength, Q factor, and BER of each multicast channel are shown in Table 1. Based on Table 1, these wavelength channels of multicasting are positioned around the central wavelength of the probe on the blue-shifted and red-shifted sides. The channel spacing is approximately 0.5 nm (e.g., from point i to point g).

Table 1. Central wavelength, Q factor, and BER of each multicast channel when pump power=300 mW, λs=1555 nm, probe power= 30 mW, λp=1545 nm, dispersion=2 ps/nm/km, and dispersion slope=0.03 ps/nm^2/km.

	Wavelength(nm)	*Q factor*	*-log(BER)*
i point	1542.45	6.15	9.59
g point	1542.95	8.79	18.36
e point	1543.47	15.59	54.60
c point	1543.99	16.18	58.70
a point	1544.49	17.13	65.53
probe	1545	21.33	100.61
b point	1545.52	26.35	153.28
d point	1546.02	17.41	67.65
f point	1546.53	9.19	19.88
h point	1547.05	6.29	9.91

The eye diagrams of the different channels are shown in Fig. 10, which illustrates that the channels that are nearer the probe wavelength lead to better wavelength-converted signal quality. One possible reason for this finding is that the channels near the wavelength of the probe have relatively higher optical power, and the channels away from the wavelength of the probe have relatively lower optical power.

Next, we perform 5/100, 7.5/100, 10/100, 15/100, 10/200, 15/200, 20/200, 30/200, 20/300, 30/300, 35/350, 40/450, and 50/500 simulations [note that the numerator is the probe power (mW) and the denominator is the pump power (mW)]. The results demonstrate that XPM is strengthened with increasing input powers. In addition, the number of multicasting channels with $Q \geq 6$ reaches 10,

which eventually decline. Figure 11 shows the relationship between the number of multicasting channels and input powers. The optical spectra of 50/500 are shown in Fig. 12, indicating that further increase in input powers will reduce the signal-to-noise ratio, which leads to the number of multicasting channels reduction.

The bandwidth of the BPF also affects the wavelength-converted signal quality. Table 2 summarizes the Q factors and BERs of a multicast channel at 1544.49 nm when the bandwidth of an optical BPF is changed from 0.10 nm to 0.26 nm. The results show that the optical filtering bandwidth of 0.16 nm to 0.2 nm is appropriate, because the BPF needs an enough bandwidth to pass a 10Gbit/s optical NRZ signal. However, a too wide bandwidth can lead to the more noise and crosstalk into the multicast channel.

Table 2 BERs and Q factors of a multicast channel at 1544.49 nm for different bandwidths of an optical BPF

Bandwidth (nm)	*Q factor*	*-log(BER)*
0.10	13.11	39.14
0.13	16.48	60.89
0.16	17.23	66.35
0.19	17.18	65.94
0.20	17.13	65.53
0.23	16.92	64.04
0.26	16.79	63.11

3.2 Simulation case 2: Dispersion=2 ps/nm/km, dispersion slope=0.03 ps/nm^2/km, λs=1560 nm, and λp=1540 nm

Figure 13 shows the optical spectra of the 1560 nm pump light with power of 300 mW and the 1540 nm probe light with power of 30 mW after the HNLF (point B in Figure 1). At least five peaks are prominent; these peaks are marked as points (a), (b),(c), (d), and (e). Six multicast channels can be obtained with their Q factors being larger than six. Comparing Figs. 8, 9, and 13, the central wavelength and the channel spacing can be affected by the wavelengths of the probe and the pump. The central wavelength, Q factor, and BER of each multicast channel are shown in Table 3. The results are similar to those in Table 1, except that the channel spacing is about 1 nm [e.g., from point (e) to point (c)].

Table 3. Central wavelength, Q factor, and BER of each multicast channel for pump power=300 mw, λs=1560 nm, probe power=30 mw, λp=1540 nm, dispersion=2 ps/nm/km, and dispersion slope=0.03 ps/nm^2/km.

	Wavelength(nm)	*Q factor*	*-log(BER)*
(e) point	1536.97	9.904	22.87
(c) point	1537.96	17.07	65.12
(a) point	1538.98	12.80	37.33
probe	1540	7.98	15
(b) point	1541	18.85	79
(d) point	1542.03	6.00	9.26

The converted signals of 1540 nm in the time domain are shown in Fig. 14. Comparing Figs. 4 and 14, the former shows that the converted signals are based on approximately 14 mW power. That is,

some direct-current power of the probe light actually adds more background noise to the channel. Therefore, Tables 1 and 3 show that the Q factor is relatively lower at the probe wavelength. The eye diagrams of different channels are shown in Fig. 15.

All the above-mentioned results are obtained under the condition that λp and λs are roughly symmetrical with approximately zero dispersion point. Furthermore, these two parameters are relatively far from the zero dispersion point. Alternately, FWM will occur.

3.3 Simulation case 3: Dispersion=5 ps/nm/km, dispersion slope=0.03 ps/nm^2/km, λs=1555 nm, and λp=1545 nm

When the dispersion is increased to 5 ps/nm/km, more neatly positioned channels are noted in Fig. 16 than in Fig. 9. Comparing Tables 1 and 4, the Q factors generally decline, and the performance differences between the channels become small.

Table 4. Central wavelength, Q factor, and BER of each multicast channel when pump power=300 mW, λs=1555 nm, probe power=30 mW, λp=1545 nm, dispersion=5 ps/nm/km,and dispersion slope=0.03 ps/nm^2/km

	Wavelength(nm)	*Q factor*	*-log(BER)*
i point	1542.43	6.28	9.96
g point	1542.95	7.93	15.23
e point	1543.45	10.21	24.29
c point	1543.98	12.04	33.20
a point	1544.49	18.49	76.17
probe	1545	9.63	21.56
b point	1545.52	10.78	26.94
d point	1546.03	9.49	21.20
f point	1546.53	7.11	12.51
h point	1547.05	6.27	9.99

3.4 Simulation case 4: Dispersion=2 ps/nm/km, dispersion slope=0.07 ps/nm^2/km, λs=1555 nm, and λp=1545 nm

When the dispersion slope is increased to 0.07 ps/nm^2/km, Fig. 17 shows asymmetrical channels on the red-shifted and the blue-shifted sides. The central wavelengths and Q factors are shown in Table 5. Only five multicast channels can be obtained with their Q factors being larger than six. When the dispersion slope becomes higher, the datum quality deterioration is critical at 1545 and 1544.49 nm, and the multicastings are degraded.

The above results suggest that we should select the HNLF that has slightly higher dispersion and slightly lower dispersion slope to support AOWC with multicasting.

Table 5. Central wavelength, Q factor, and BER of each multicast channel when pump power=300 mW, λs=1555 nm, probe power=30 mW, λp=1545 nm, dispersion=2 ps/nm/km, and dispersion slope=0.07 ps/nm^2/km

	Wavelength(nm)	*Q factor*	*-log(BER)*
h point	1542.44	2.75	2.55
g point	1542.95	7.38	13.25
e point	1543.45	15.51	54.08
c point	1543.97	21.20	99.52
a point	1544.49	3.14	4.22
probe	1545	3.36	3.91
b point	1545.51	25.07	138.46
d point	1546.03	6.98	12.05
f point	1546.54	2.99	2.91

4. Conclusions

AOWC with multicasting is investigated in this paper, which is based on XPM in a HNLF. With a pump-modulated light and only a single CW probe, wavelength multicasting is realized by appropriately controlling the powers of two beams. Ten multicast channels can be obtained with $Q \geq 6$ and the channel spacing is approximately 0.5nm when the probe and pump wavelengths are 1545 nm and 1555 nm, respectively; Six multicast channels can be obtained with $Q \geq 6$ and the channel spacing is approximately 1 nm when the probe and pump wavelengths are 1540 nm and 1560 nm, respectively. The performance of multicast channels can be affected by the dispersion and the dispersion slope of a HNLF.

References

[1] E. Ciaramella, "Wavelength conversion and all-optical regeneration: Achievement and open issues," *J. Lightw. Techno*. vol. 30, no. 4, pp. 572-580, 2012

[2] S. J. B. Yoo, "Wavelength conversion technologies for WDM network applications," *J. Lightw. Technol.*, vol. 14, pp. 955–966, 1996.

[3] M. Koga, Y. Hamazumi, A. Watanabe, S. Okamoto, H. Obara, K.-I. Sato, M. Okuno, and S. Suzuki, "Design and performance of an optical path cross-connect system based on wavelength path concept," *J. Lightwave Technol.*, vol. 14, pp. 1106-1119, 1996.

[4] Y. Wang, C. Yu, T. Luo, L. Yan, Z. Pan, and A.E. Willner, "Tunable all-optical wavelength conversion and wavelength multicasting using orthogonally polarized fiber FWM," *J. Lightwave Technol.*, vol. 23, no. 10, pp. 3331-3338, 2005.

[5] B.-E. Olsson, P. Ohlen, L. Rau, and D.J. Blumenthal, "A simple and robust 40-Gb/s wavelength converter using fiber cross-phase modulation and optical filtering," *IEEE Photon. Tech. Lett.*, vol. 12, no. 7, pp. 846-848, 2000.

[6] J. H. Lee, T. Nagashima, T. Hasegawa, S. Ohara, N. Sugimoto, T. Tanemure, and K. Kikuchi, "Wavelength conversion of 40-Gbit/s NRZ signal using four-wave mixing in 40-cm-long Bismuth oxide based highly-nonlinear optical fiber," in Technical Digest of 2005 *Optical Fiber Communications Conference*, paper PDP23, Anaheim, USA, 6-11 March 2005.

[7] R. K. Pankaj, "Wavelength requirements for multicasting in all-optical networks," *IEEE/ACM*

Trans. Network., vol. 7, pp. 414–424, 1999.

[8] K. K. Chow, Chester Shu, Chinlon Lin, Anders Bjarklev, "All-optical wavelength multicasting with extinction ratio enhancement using pump-modulated four-wave mixing in a dispersion-flattened nonlinear photonic crystal fiber," *IEEE J. Sel. Topics Quantum Electron.*, vol. 12, no. 4, pp. 838-842, 2006.

[9] N. Yan, E. Tangdiongga, H. D. Jung, I. Tafur Monroy, H. de Waardt, A. M.J. Koonen, "Regenerative all-optical wavelength multicast for next generation WDM network and system applocations," *Photon. Netw. Commun.*, vol. 15, pp. 1-6, 2008.

[10] W. Astar , J. B. Driscoll, Xiaoping Liu, J. I. Dadap, W. M. J. Green, Y. A. Vlasov, G. M. Carter, R. M. Osgood, "Tunable wavelength conversion by XPM in a silicon nanowire, and the potential for XPM-multicasting," *J. Lightwave Technol.*, vol. 28, no. 17, pp. 2499-2511, 2010.

[11] M.P. Fok and C.S. Shu, "Multipump four-wave mixing in a photonic crystal fiber for 6×10 Gb/s wavelength multicasting of DPSK signals," *IEEE Photon. Tech. Lett.*, vol. 19, no. 15, pp. 1166-1168, Aug. 2007.

[12] Z.-Q. Hui and J.-G. Zhang, "Wavelength conversion, time demultiplexing and multicasting based on cross-phase modulation and four-wave mixing in dispersion-flattened highly nonlinear photonic crystal fiber," *J. Opt.*, vol. 14, no. 5, 055402 (8pp), 2012.

[13] Zhan-Qiang Hui, Jian-Guo Zhang et al., "Demonstration of 40 Gbit/s all-optical return-to-zero to nonreturn-to-zero format conversion with wavelength conversion and dual-channel multicasting based on multiple cross-phase modulation in a highly nonlinear fiber," *Opt. Eng*, vol. 52, pp. 055002, 2013

[14] P. Mehta, N. Healy, T. D. Day, J. V. Badding, A. C. Peacock, "Ultrafast wavelength conversion via cross-phase modulation in hydrogenated amorphous silicon optical fibers," *Opt. Express* vol. 24, pp. 261110-26116, 2012

[15] http://www.oelabs.com/images/goodspdf/201109/High%20Nonlinear%20Optical%20Fibre.pdf

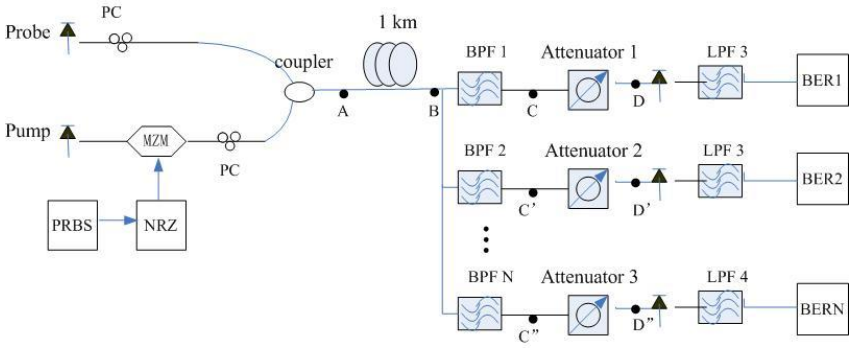

Fig. 1. Simulation experiment for XPM-based AOWC with multicasting.

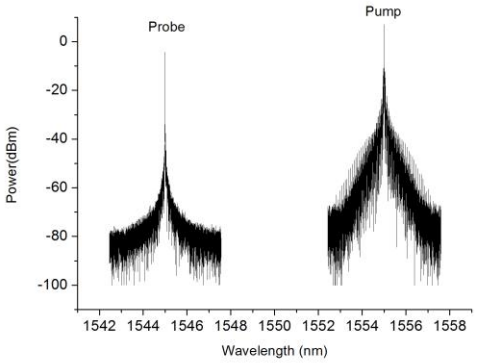

Fig. 2. Optical spectra of pump power=45 mW, λs=1555 nm, probe power=1 mW, and λp=1545 nm before the HNLF.

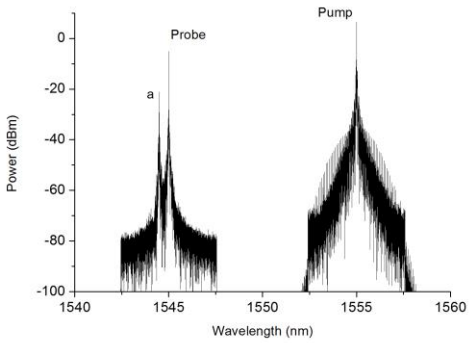

Fig. 3. Optical spectra of pump power=45 mW, λs=1555 nm, probe power=1 mW, and λp=1545 nm after the HNLF.

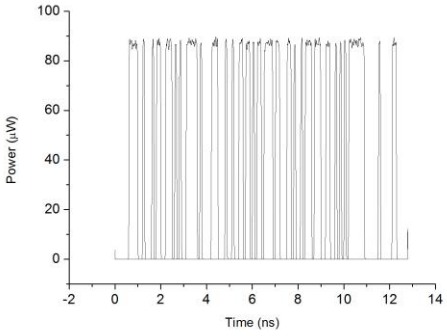

Fig. 4. The wavelength-converted signal after BPF at 1544.49 nm in time domain.

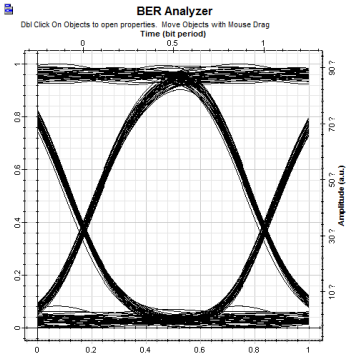

Fig. 5. The eye diagram at 1544.49 nm.

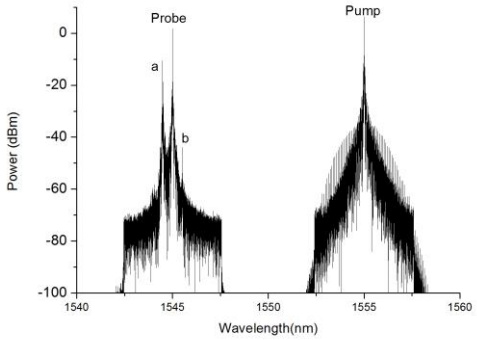

Fig. 6. Optical spectra at pump power=45 mW, λs=1555 nm, probe power=5 mW, and λp=1545 nm after the HNLF..

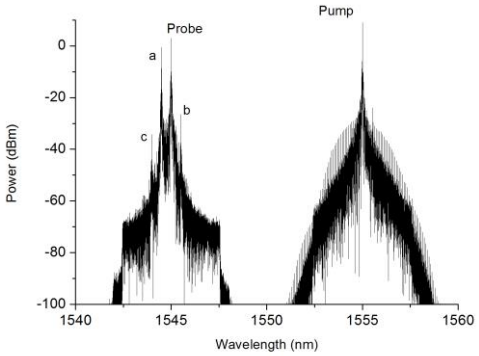

Fig. 7. Optical spectra at pump power=100 mW, λs=1555 nm, probe power=10 mW, and λp=1545 nm after the HNLF.

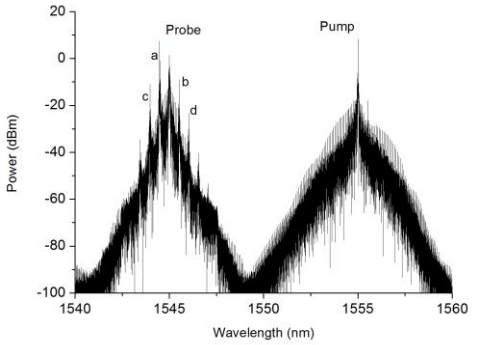

Fig. 8 Optical spectra at pump power=200 mW, λs=1555 nm, probe power= 20 mW, and λp=1545 nm after the HNLF.

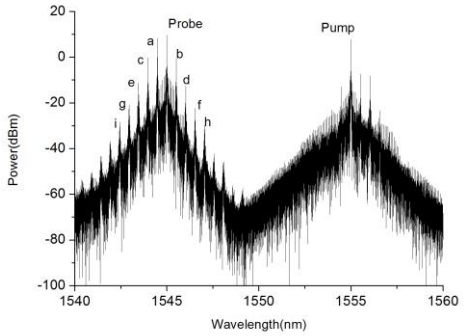

Fig. 9. Optical spectra at pump power=300 mW, λs=1555 nm, probe power=30 mW, and λp=1545 nm after the HNLF.

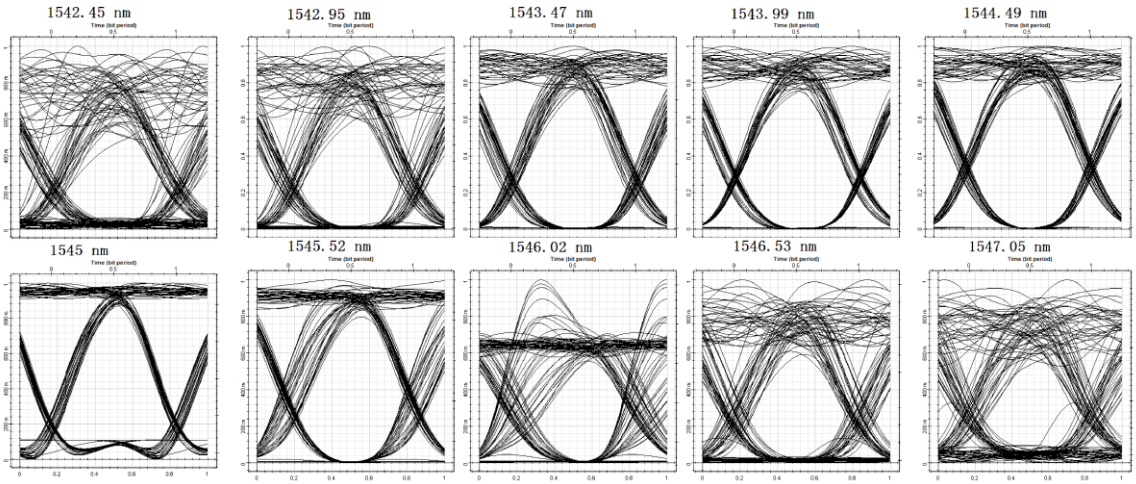

Fig. 10. The eye diagrams of different channels at λs = 1555 nm and λp = 1545 nm.

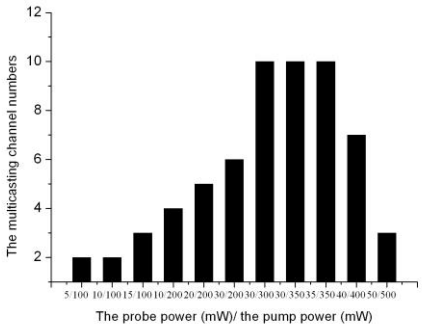

Fig. 11. The relationship between input powers and the number of multicasting channels with $Q \geq 6$.

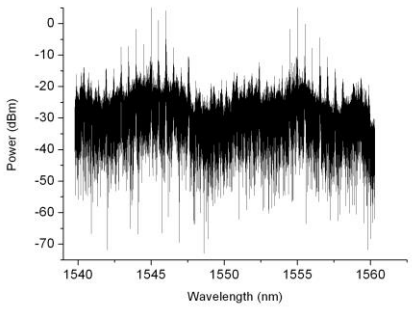

Fig. 12. Optical spectra at pump power=500 mW, λs=1555 nm, probe power=50 mW, and λp=1545 nm after the HNLF.

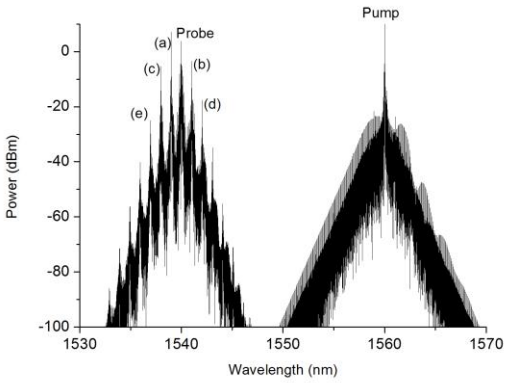

Fig. 13. Optical spectra at pump power=300 mW, λs=1560 nm, probe power=30 mW, and λp=1540 nm after the HNLF.

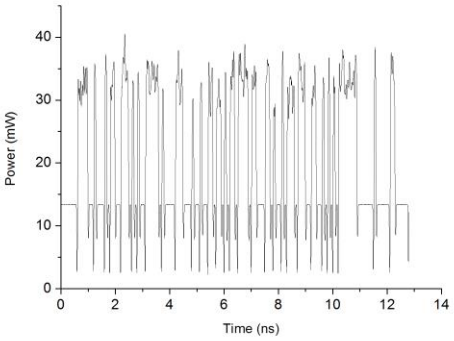

Fig. 14. The converted signal after BPF at 1540 nm in time domain.

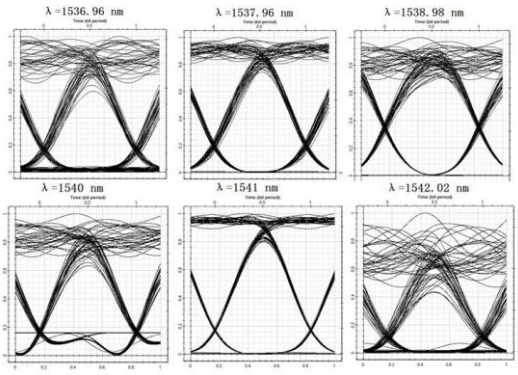

Fig. 15. The eye diagrams of different channels at λp=1540 nm and λs=1560 nm.

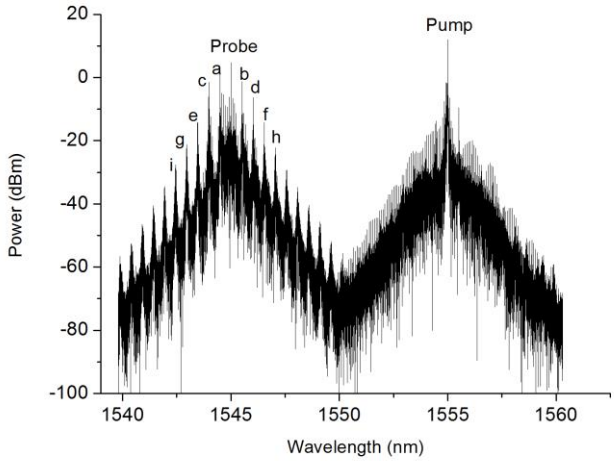

Fig. 16. Optical spectra at pump power=300 mW, λ*s*=1555 nm, probe power=30 mW, λ*p*=1545 nm, dispersion=5 ps/nm/km, and dispersion slope=0.03 ps/nm^2/km after the HNLF.

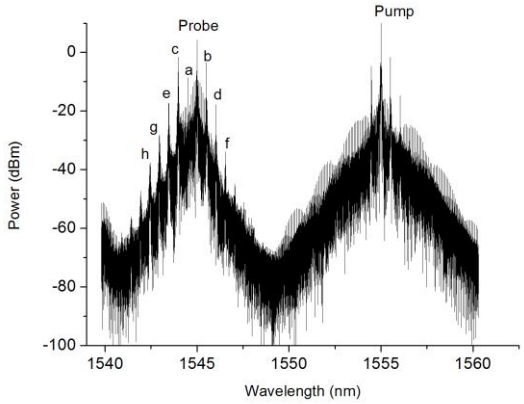

Fig. 17. Optical spectra at pump power=300 mW, λ*s*=1555 nm, probe power=30 mW, λ*p*=1545 nm, dispersion=2 ps/nm/km, and dispersion slope=0.07 ps/nm^2/km after the HNLF.